AN OPERATIONAL SYSTEM FOR SENSOR MODELING AND DEM GENERATION OF SATELLITE PUSHBROOM SENSOR IMAGES

Y. Wang*, X. Yang, F. Xu, A. Leason, S. Megenta

ERDAS, Inc., 5051 Peachtree Corners Circle, Suite 100, Norcross, GA 30092, USA
younian.wang@erdas.com

Commission I, WG I/5

KEY WORDS: Sensor, Modeling, Triangulation, Image, Matching, DEM, Extraction, Pushbroom

ABSTRACT:

This paper introduces an operational and extensible system for sensor modeling, triangulation, DEM extraction and stereo mapping of space borne pushbroom sensor images. The methods for sensor modeling and triangulation are introduced with the consideration of the newer sensors such as EROS A1, ALOS PRISM, FORMOSAT2 and THEOS satellite systems. They are based on the collinearity equation and bundle block adjustment. The orbital ephemeris data are rigorously considered. They are equally applicable for SPOT5, QuickBird and GeoEye images. In case pushbroom sensor images are provided with rational functional model without the specifications of the sensor, an additional correction triangulation will be performed using polynomial model. Test results with real data are presented and a comparison between these two models is carried out. Problems associated with automatic extraction of a DEM from high resolution satellite images are investigated and an adaptive feature based image matching method is introduced. The results from several datasets show the good quality and efficiency of the proposed method. Together with the introduced algorithms and techniques, and rigorous software engineering requirements and standard a software system is built for mapping with high resolution satellite images with easy extensibility for new similar sensors. Several examples show the superior performance and high quality of the system and developed technology.

1. INTRODUCTION

Nowadays high resolution space borne optical imagery is available from a variety of platforms and specifications. The older generation includes SPOT, IRS-1C, IKONOS, ORBIMAGE OrbView 2 and QuickBird, the newer sensors are SPOT 5, ASTER, EROS, ALOS PRISM, GeoEye OrbView 3, QuickBird WorldView, CARTOSAT and FORMOSAT2 etc. Another new addition to this family is the Thailand's THEOS, which is planned to launch at the end of June 2008 in most recent schedule. All these sensors deliver pushbroom type of images with nominal ground resolution from half a meter to about 10 meters in the highest resolution band (normally the panchromatic channel). Some of them offer along-track stereo capability, while others provide images with cross-track overlap from two adjacent orbits. Because of their high resolution, stable geometry and stereo capability, mapping the Earth from these images is becoming more and more production workflow rather than a research activity.

In order to take the full potential of these images advanced algorithms and methods have to be developed and applied in the processing systems. In the past decade, a lot of research has been carried out for the optimal photogrammetric processing of high resolution satellite images, especially in the area of sensor modeling and triangulation, automatic digital terrain model extraction and 3D mapping potentials. For example, Fritsch & Stallmann (2000) presented a complete triangulation solution for processing high resolutions pushbroom images. Fraser & Hanley (2003), Grodecki & Dial (2003) and Niu et al (2004) have reported methods to improve rational function model (RPC) accuracy. Jacobsen (2007) has given a through overview about orientation methods for space borne images. Pateraki & Baltsavias (2003) have investigated image matching methods for pushbroom sensor images. Buyuksalih & Jacobsen (2004) investigated the methods and quality of generating DEMs from high resolution space borne images.

Based on the research results of the academic community and our internal research achievements, ERDAS Inc. has developed a complete solution for processing various kinds of satellite pushbroom images and included it in its well-known and most widely used photogrammetric software product LPS. This world-class software keeps improving and perfecting continuously since it is first released in 2004. Some early features and performance can be found in (wang, et al, 2004). In this paper the methods for sensor modeling and triangulation, and automatic DTM extraction for high resolution space borne images are described. The availability and quality of various kinds of satellite pushbroom images are introduced. Many examples are presented to show the capability and accuracy of the data and the effectiveness of the LPS algorithms. Stereoscopic mapping and 3D feature collection from high resolution space borne pushbroom images are also strong features of LPS, but they will be introduced in a separate paper.

2. SENSOR MODELING AND TRIANGULATION

Even though there are many satellite pushbroom sensors in operation, each pushbroom image normally consists of a certain number of scan lines, and each scan line is a perspective projection and follows the collinearity equation. For the purposes of photogrammetric mapping the most suitable level

* Corresponding author.

of images is the radiometrically corrected, geometrically raw images. They are normally called level I images, such as SPOT Scene level 1A images and ALOS PRISM 1A/1B images. Although LPS can also process some geometrically processed images, the discussion about sensor modeling and triangulation below will be limited to the image level without geometric correction.

Generally speaking, high resolution satellite pushbroom images are delivered in 3 categories in terms of geometry and orientation information. The first category is images that are delivered together with rational polynomial coefficients (RPC). This category includes IKONS RPC, QuickBird RPC, NITF RPC, RESOURCESAT RPC, ALOS RPC etc. The second category is images that are delivered with metadata or DIMAP files, which contain the satellite ephemeris information including position, velocity and altitude of the satellite (sensor) during the image acquisition. Many satellite pushbroom sensor owners provide image data in this category, such as SPOT 5, ASTER, EROS, ALOS PRISM, FORMOSAT 2, THEOS, GeoEye OrbView and QuickBird WorldView. The third category is the older generation satellite pushbroom sensors, such as SPOT and IRS-1C. Images in this category are usually only attached with a simple header file where only some general information about the sensor and image is included such as orbit height, focal length, viewing angles, time and location. No detailed orientation information is available in this category.

2.1 RPC model refinement

For images with a RPC model, sensor specific information such as sensor type, focal length and principle point is not known. Instead a group of rational function coefficients are attached to describe the relationship of an image point to its corresponding ground point. As showed in the following equation:

$$x = \frac{P_1(X,Y,Z)}{P_2(X,Y,Z)} \qquad y = \frac{P_3(X,Y,Z)}{P_4(X,Y,Z)} \tag{1}$$

Where (x, y) is image pixel coordinates, (X,Y,Z) is ground coordinates in a certain map coordinate system such as geographic coordinates or UTM. $P_i(X,Y,Z)$ is polynomial function of point (X,Y,Z), normally a 3rd order polynomial with 20 coefficients for each function:

$$\begin{aligned} P_i(X,Y,Z) = {} & a_{i0} + a_{i1}X + a_{i2}Y + a_{i3}Z + a_{i4}X^2 + a_{i5}XY + \\ & a_{i6}Y^2 + a_{i7}YZ + a_{i8}XZ + a_{i9}Z^2 + a_{i10}X^3 + \\ & a_{i11}X^2Y + a_{i12}X^2Z + a_{i13}XY^2 + a_{i14}XZ^2 + \\ & + a_{i15}Y^3 + a_{i16}Y^2Z + a_{i17}YZ^2 + a_{i18}Z^3 + \\ & a_{i19}XYZ \end{aligned} \tag{2}$$

Where i = 1, 2, 3, or 4, representing 4 different polynomials respectively.

Since these polynomial coefficients are usually computed from the sensor information and satellite ephemeris data, they are not accurate enough for photogrammetric mapping. How to improve the accuracy of RPC model was an interesting topic for many researchers. Among them Fraser & Hanley (2003) recommend an affine bias correction of image coordinates. A 3D affine correction of ground coordinates can be also an option (Niu et al, 2004).

In LPS an additional polynomial correction to the image points is introduced to the sensor model, as shown in following equation:

$$x + f_1(x,y) = \frac{P_1(X,Y,Z)}{P_2(X,Y,Z)} \qquad y + f_2(x,y) = \frac{P_3(X,Y,Z)}{P_4(X,Y,Z)} \tag{3}$$

Where f(x, y) can be zero order, 1st order or 2nd order polynomial depending on user's choice and number of ground control points (GCP). Its form is shown below:

$$f_1(x,y) = a_0 + a_1x + a_2y + a_3x^2 + a_4xy + a_5y^2 \qquad f_2(x,y) = b_0 + b_1x + b_2y + b_3x^2 + b_4xy + b_5y^2 \tag{4}$$

It is merely a shift with order 0 and 2D affine when order 1. Each parameter can be individually weighted. By setting a specific weight a particular parameter can be kept at certain value or excluded from the model. A bundle block adjustment will be performed to solve these parameters. A benefit of using this simple polynomial model is that it can start improving the RPC model when there is only one GCP available. When there are more GCPs, more parameters can be included with the aim of compensating for more systematic errors contained in RPCs.

Table 1 shows the root mean square errors of check point image residuals from two production datasets. For the privacy of the data providers, no platform names are listed here. We can see the original RPC model has significant errors, here 80 pixels and 20 pixels respectively. With just 1 or 2 GCPs, the error can be reduced to about 1/10 to 1/20 of the original error level. Another interesting point can be found here that higher order polynomial does not necessarily increase the accuracy. This is in line with one test showed in (Niu et al, 2004). The reason may be related to the fact that the GCPs are not accurate here, they are in a few pixels range. Further investigation may reveal more explanations. Even though the residuals are still at 2 to 3 pixel level after the refinement (because of the limited quality of GCPs and the dataset itself), the refined model can offer satisfactory stereo viewing, DTM collection and orthoimage procession. Therefore this refinement step is very helpful and necessary.

$rmse = \sqrt{(rx^2 + ry^2)/2n}$		check point RMSE (pixels)		
		0 order	1st order	2nd order
data set I: check points n=3	No Refine	79.17		
	1 GCP	4.88		
	3 GCPs	3.80	3.93	
data set II: check points n=5	No Refine	20.89		
	2 GCPs	2.40		
	4GCPs	1.91	2.48	
	6 GCPs	1.87	2.24	2.28

Table 1. Check point residual RESE of RPC refinement

2.2 Orbital Pushbroom Model with Ephemeris Data

The newer satellite pushbroom image providers deliver images with metadata files which include detailed sensor parameters and sensor location, velocity and attitude information. These data come from the on-board location and attitude measurement and control systems such as Star Tracker, Gyro, GPS and Sun sensor. These data can be quite accurate, but normally need to be converted to photogrammetric exterior and interior orientation for photogrammetric modeling and mapping purposes. The conversion can be related to a series of coordinate systems including image pixel coordinate system, camera coordinate system, satellite body coordinate system, orbital coordinate system, Earth centred inertial (ECI) system, Earth centred Fixed (ECF) coordinate system, and Geodetic system. Many ephemeris data providers already provide sensor location, velocity and attitude in ECF system, such as SPOT 5 and QuickBird. Then the metadata parser only needs to convert the data from ECF to Geodetic and then to a local tangent space rectangular (LSR) coordinate system. Some other image providers deliver ephemeris data based on ECI system, such as EROS, FORMOSAT 2 and THEOS. In this case, the metadata parser has to convert firstly the location and/or attitude data from ECI to ECF system.

ECI coordinate to ECF coordinate conversion involves 4 rotations, namely rotations caused by Sidereal time, notation, precession and polar motion. For space saving purposes, these conversion equations are omitted here. Details can be found in Technical Notes of International Earth Rotation and Reference Systems Service (IERS) at http://www.iers.org. Furthermore attitude data are normally delivered in quaternion with 4 parameters q_1, q_2, q_3 and q_4. These need to be converted to conventional omega, phi, and kappa through the rotation matrix. Once these preparations are finished, image exterior orientation parameters are available as a function of time t.

Since each line of a pushbroom sensor image is still a central perspective projection, the image point and its corresponding ground point meet the collinearity equation:

$$\begin{bmatrix} x - p_x \\ -p_y \\ -f \end{bmatrix} = \lambda \cdot M \cdot \begin{bmatrix} X - X_s \\ Y - Y_s \\ Z - Z_s \end{bmatrix} \quad (5)$$

Where x is the image coordinate in the line, (X,Y,Z) is the ground coordinate, p_x, p_y is the principal point, f is the focal length. Rotation matrix M from omega (Os), phi (Ps), kappa (Ks) and projection centre (Xs, Ys, Zs) can be assumed from the ephemeris data after the conversion.

Since the exterior orientation (Xs, Ys, Zs, Os, Ps, Ks) from ephemeris data may not be accurate enough, we use the following model for additional adjustment when GCPs are available:

$$\begin{bmatrix} x - p_x \\ -p_y \\ -f \end{bmatrix} = \lambda \cdot \Delta M \cdot M \cdot \begin{bmatrix} X - X_s - \Delta X_s \\ Y - Y_s - \Delta Y_s \\ Z - Z_s - \Delta Z_s \end{bmatrix} \quad (6)$$

Where additional rotation matrix ΔM and (ΔXs, ΔYs, ΔZs) represent the additional correction to the ephemeris exterior orientation. Depending on the available number of GCPs and the accuracy of ephemeris data, the exterior orientation correction can be as simple as a shift, or higher order polynomials. Each parameter can have different orders and weights. A bundle block adjustment will be performed to optimally determine the orientation correction parameters and the ground point coordinates.

The following table shows results from several datasets. They are from different pushbroom sensors. For the same privacy reason, no specific name is listed here. The table lists root mean square errors of check points for x and y coordinates separately, and the point RMSE which equals:

$$RMSE(pt) = \sqrt{RMSE^2(x) + RMSE^2(y)} \quad (7)$$

Data Source		check point RMSE (pixels)		
		RMSE(x)	RMSE(y)	RMSE(Pt)
Dataset I check points n=5	No GCP	31.85	71.99	78.72
	3 GCPs	1.79	2.01	2.75
	7 GCPs	1.73	1.18	2.10
	13 GCPs	0.69	0.95	1.18
Dataset II check points n=6	No GCP	39.28	1214.05	1214.68
	3 GCPs	24.75	22.95	33.75
	6 GCPs	1.04	3.03	3.20
	9 GCPs	0.76	2.16	2.29
Dataset III check points n=4	No GCP	16.91	32.92	37.01
	3 GCPs	0.41	3.25	3.28
	6 GCPs	0.39	1.03	1.10
	9 GCPs	0.37	0.96	1.03
Dataset IV check points n=4	No GCP	2.67	8.65	9.05
	3 GCPs	0.97	0.57	1.13
	6 GCPs	0.49	0.82	0.96
	9 GCPs	0.54	0.59	0.80

Table 2. Check point residuals of orbital pushbroom model

From table 2 we can summarize a few interesting points:

1. Accuracy is worse in flight direction (y direction) when only ephemeris data is used (no GCP case).
2. Ephemeris data accuracy can vary greatly from sensor to sensor, and from dataset to dataset.
3. With just a few GCPs the orientation accuracy can be improved significantly with the described sensor modeling method.
4. Comparing to table 1, it looks like the introduced orbital pushbroom model can achieve higher accuracy than the RPC refinement model. This point need be further investigated for verification.

2.3 Generic Pushbroom Sensor Model

Some older satellite pushbroom scanners provide images without detailed ephemeris data or RPCs. They provide simply the images and some basic parameters about the scanner such as focal length, nominal flight height, along track and across track viewing angles. For example, SPOT and IRS-1C provide this type of image products. In this case a generic pushbroom sensor model will be used, which still describes each scan line with collinearity equation, and the exterior orientation parameters will change with time in polynomial form, as showing below:

$$\begin{bmatrix} x - x_0 \\ 0 \\ -f \end{bmatrix} = \lambda \cdot M(\omega, \varphi, \kappa) \cdot \begin{bmatrix} X - X_S \\ Y - Y_S \\ Z - Z_S \end{bmatrix} \quad (8)$$

With:

$$\begin{aligned} X_S &= x_0 + a_1 * t + a_2 * t^2 + \cdots \\ Y_S &= Y_0 + b_1 * t + b_2 * t^2 + \cdots \\ Z_S &= Z_0 + c_1 * t + c_2 * t^2 + \cdots \\ \omega &= \omega_0 + d_1 * t + d_2 * t^2 + \cdots \\ \varphi &= \varphi_0 + e_1 * t + e_2 * t^2 + \cdots \\ \kappa &= \kappa_0 + f_1 * t + f_2 * t^2 + \cdots \end{aligned} \quad (9)$$

Where ai, bi, ci etc. are polynomial coefficients. Unlike RPC refinement model or Orbital Pushbroom model, you have to have enough GCPs to solve the model in order to get ground coordinates. Also it requires much more GCPs to reach the comparable level of accuracy as the previous two models. Examples for this model are omitted here.

3. AUTOMATIC DTM EXTRACTION

Once image orientation is solved through the sensor modeling methods introduced in the previous section, the high resolution satellite pushbroom scanner images can be used for automatic DTM extraction with image matching algorithms. Most DTM matching techniques and algorithms for traditional aerial images can still be used for high resolution space borne images. There are some specialities of space borne pushbroom sensor images. They have lower ground resolution (GSD) than high resolution airborne images, so less detail is contained in the image. Sometimes this is advantageous for image matching algorithms. On other hand, space borne images are normally darker than air borne images mainly because of the shorter exposure time. This leads to lower contrast which is normally a disadvantage for image matching. The amount of image parallax is still the decisive factor for determining the search range when doing matching with satellite pushbroom images. The amount of image parallax is still dependent on the base to height ratio and the terrain variation (elevation range). For cross track image pairs, the base line is usually small compared to the satellite height, thus the image parallax is also small. For along track stereo pairs, depending on the backward and forward looking angles, sometimes the base to height ratio can be large. For example, ALOS PRISM backward and forward image pair has a base to height ratio of 1. Image matching algorithms have to consider these changing dynamics of various base to height ratios and adapt the image search range for matching accordingly.

ERDAS LPS has used a feature based, automatic terrain adaptive, hierarchical image matching scheme for automatic DTM extraction. A global DTM at the resolution of 30 seconds is distributed and used for the initial terrain analysis and adaptive parameter initialization. Customer's own DTM can also be used for this purpose. After matching on each pyramid level the terrain will be refined, gross error will be removed and a more accurate and detailed terrain serve as the input of next pyramid level correlation.

Two examples will be displayed and analyzed in the following paragraphs. The first example is an EROS A1 image pair covering a mountainous area of approximately 14km x 15km in Switzerland. The ground pixel size is about 2 meters. The images look pretty dark and have some cloud in the centre. Figure 1 shows the original image pair. Figure two shows the automatically extracted DEM. Checking with a stereoscopic view of the image pair, it can be seen the the DEM in the most part is very good, but the cloud area has produced some incorrect matches, as showed in the lower right corner of Figure 2 and Figure 3. Figure 3 shows the 3D view of the image by rendering it on top of the DEM with perspective display.

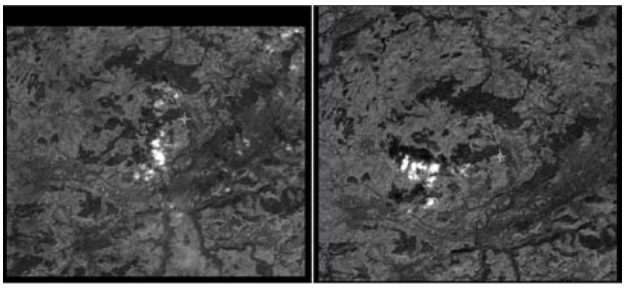

Figure 1. An EROS A1 image pair

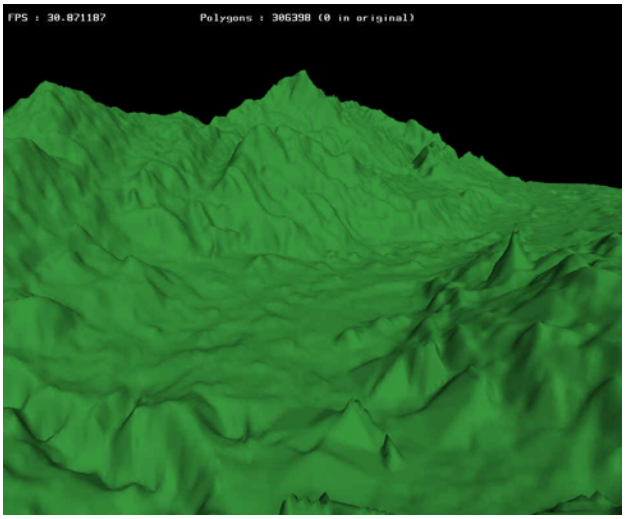

Figure 2. Automatic DEM from the EROS A1 image pair

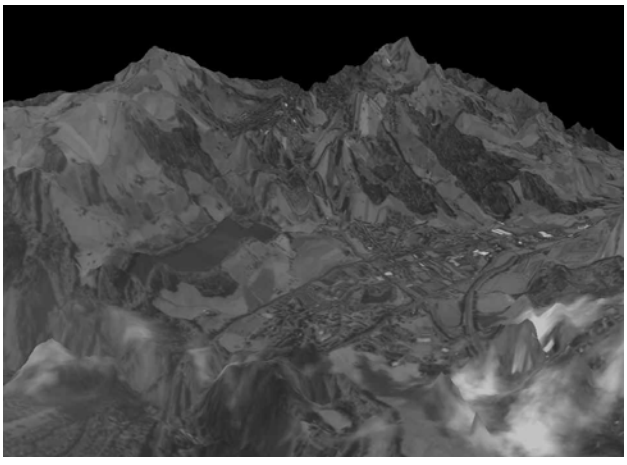

Figure 3. 3D view of the EROS A1 image (part)

The second example is an ALOS PRISM dataset, which contains 3 panchromatic images with along track stereo. Figure 4 shows the nadir image. The both forward image and backward image have over 84% overlap with the nadir image. Figure 5 shows the triangulation report for the 3 ALOS images. There are only 4 ground points digitized from 1:25,000 topographic map. We use 2 as control points, and another 2 as check points. Considering the low number and quality of control points, we think the 4 pixel check point root mean square is reasonable. Figure 6 shows the automatically extracted DEM from all 3 images. Figure 7 shows the 3D view of the nadir image by overlaying the oriented image on top of the DEM with perspective display. From Figure 6 one can see that the water body caused no matches to be found in the upper middle corner. The cloud at the lower right part also caused some incorrect matches. Other than these two areas, the DEM described the terrain quite well by visual inspection.

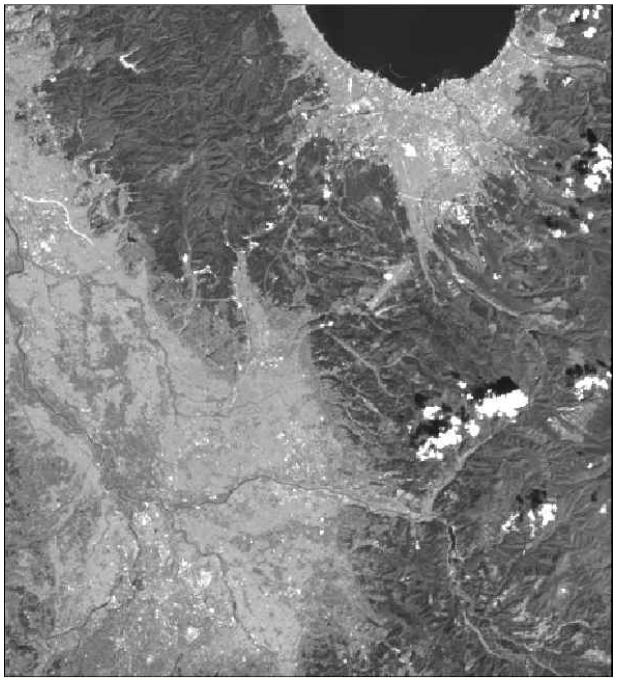

Figure 4. ALOS PRISM nadir image

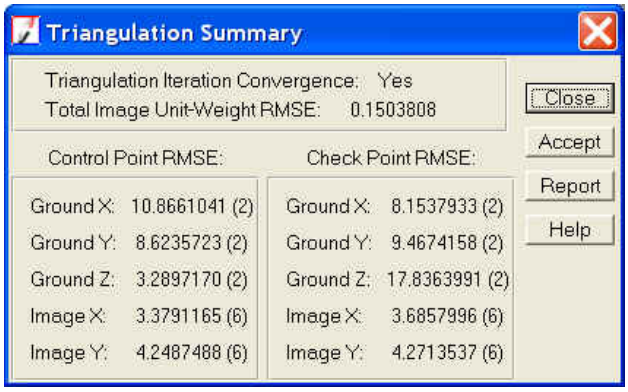

Figure 5. Triangulation report of 3 ALOS PRISM images

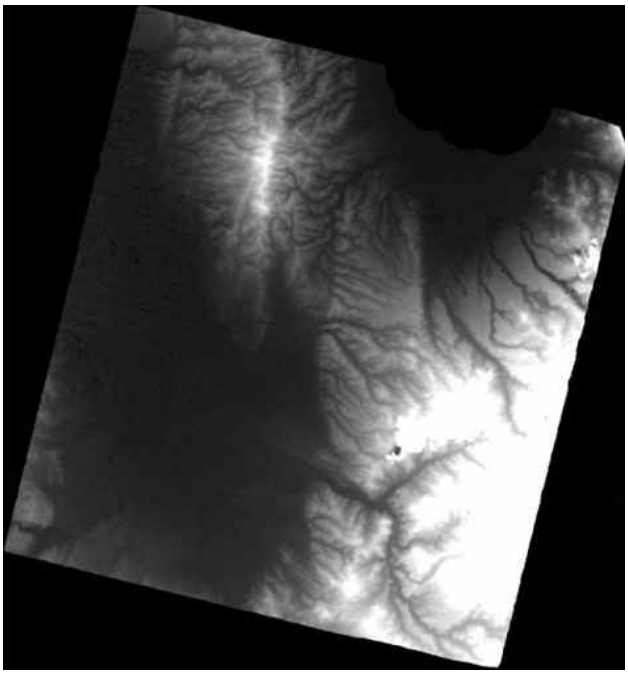

Figure 6. DEM from 3 ALOS PRISM images

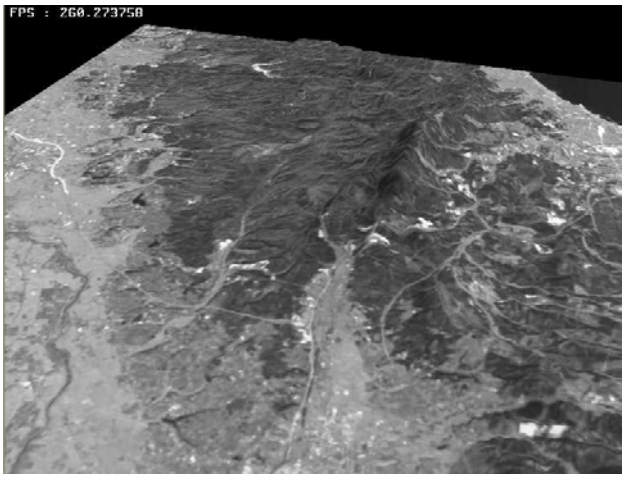

Figure 7. 3D view of ALOS PRISM nadir image (part)

Table 3 shows some general information about the tested EROS dataset and ALOS PRISM datasets shown in Figure 1 and Figure 4 and a summary of the extracted DEMs. There are 52 pre-determined ground points available for EROS dataset. We use these ground points as check points to assess the accuracy of the extracted DEM. The elevation value at the horizontal location of each check point will be interpolated from the DEM, then the difference against the check point elevation will be computed, then mean error and root mean square error are calculated. The same computation is also done for the ALOS DEM, where 69 ground check points are available. We can see from table 3 that there are a few meters difference between check point elevation and DEM elevation values. This is understandable because there are two interpolations involved here. Firstly, the DEM is interpolated from the individual matched points; secondly, the check point elevation is interpolated from DEM. The interpolated elevation will not normally sit exactly on the terrain surface. Depending on the roughness of the terrain and the density of DEM points, there is

usually some difference between the real elevation and the interpolated one. A more accurate way to check the accuracy of the extracted DTM is to choose TIN as the DTM format. After the DTM is generated, load the TIN into a stereo editor such as LPS TerrainEditor and check the matched points individually to see if they are on the terrain surface. A visual check with EROS DTM in TIN format was performed. A random sample of 110 points from the total matched DTM points were checked against their true image locations on the image pair. There were only two points for which it was not possible to determine the correct image location due to clouds on one of the images. Thus, the visual check indicated that about 98% of matched points are correct in the example.

	EROS	ALOS
Image size in pixels	6883x7490	14496x16000
Ground pixel size	1.8m	2.5m
Orbit height	480km	690km
Focal length	3540mm	1939mm
DEM cell size	20x20m	20x20m
DEM range	494 to 1059m	-38 to 1435m
Mean DEM elevation	704m	102m
Num of check points	52	69
Mean Error of check pt	1.78m	-2.31m
RMSE of check points	3.82m	6.45m

Table 3. EROS & ALOS datasets with DEM information

4. SUMMARY

This paper introduced the methods and algorithms of sensor modeling, triangulation and automatic DTM extraction for high resolution satellite pushbroom scanner images. Three sensor modeling methods are available in LPS to model space borne pushbroom images. The introduced RPC refinement method and orbital pushbroom triangulation can improve the accuracy of the images significantly, even when there are only a few GCPs available. These are necessary steps for high accuracy mapping from space borne images. The developed automatic DTM extraction method works very well for high resolution satellite pushbroom images. But the cloud on some of the space borne pushbroom images can cause wrong matches, and will be the next improvement point. The flexibility, extensibility and quality of the introduced methods guarantee their applicability to all kinds of space borne pushbroom scanner images.

ACKNOWLEDGEMENTS

The authors would like to thank Remote Sensing Technology Center of Japan (RESTEC) for kindly providing the ALOS sample data for software testing and validation.

REFERENCES

Fraser, C. S., Hanley, H. B., 2003. Bias Compensation in Rational functions for Ikonos Satellite Imagery. *Photogrammetric Engineering and Remote Sensing*, 69(1), pp. 53-57.

Grodecki J., Dial G., 2003. Block Adjustment of High-Resolution Satellite Images Described by Rational Polynomials. Photogrammetric Engineering and Remote Sensing, 69(1), pp. 59-68.

Buyuksalih, G., Jacobsen, K., 2004, Generation and Validation of High Resolution Space Image DEMS. In Proceedings of ASPRS Annual Conference, Denver, Colorado, USA.

Fritsch, D., Stallmann, D., 2000, Rigorous Photogrammetric Processing of High Resolution Satellite Imagery. In: *The International Archives of the Photogrammetry, Remote Sensing and Spatial Information Sciences*, Amsterdam, The Netherlands, Vol. XXXIII, Part B4, pp. 313-321.

Jacobsen, K., 2007, Orientation of High Resolution Optical Space Images. In Proceedings of ASPRS Annual Conference, Tampa, Florida, USA.

Niu, X., Wang, J., Di, K., Li, R., 2004, Geometric Modeling and Processing of QuickBird Stereo Images. In Proceedings of ASPRS Annual Conference, Denver, Colorado, USA.

Pateraki M., Baltsavias E., 2003, Analysis and Performance of the Adaptive Multi-image Matching Algorithm for Airborne Digital Sensor ads40. In. Proceedings of ASPRS Annual Conference, Anchorage, USA.

Wang, Y., Yang, X., Stojic, M., Skelton, B., 2004. Toward Higher Automation and Flexibility in Commercial Digital Photogrammetric System. In: *The International Archives of the Photogrammetry, Remote Sensing and Spatial Information Sciences*, Istanbul, Turkey, Vol. XXXV, Part B2, pp. 838-841.